NONSTEADY STATE PROCESSES AT PROPAGATION OF LASER BEAMS IN SELF–INDUCED CONVECTIVE FLOWS

R.Sh. Tsvyk

Institute of Atmospheric Optics,
Siberian Branch of the Russian Academy of Sciences, Tomsk
Received July 31, 1998

In this paper we present a review of the experimental results and results of simulations of nonsteady state processes that occur at laser beam propagation through media under conditions of self-induced convection. The conditions under which different regimes of convective motion and laser beam aberrations may occur, as well as time and amplitude characteristics of the image displacements are considered.

At laser beam propagation through the rest zone the nonsteady state (transient) processes connected with the establishment of convective motion (self-induced convection) in the propagation channel play a significant part. The investigations of the occurrence and development of a self-induced convective flow, distortions of the laser beam parameters, propagated through such media, are a very complicated mathematical problem since the temperature and velocity fields in a convective flow may only be defined by integration of the hydrodynamics equations. Analysis of convection, induced by a laser beam, has been described in Refs. 1–3, 6, 7, and 11, and the problems of laser beam propagation in Refs. 2 to 12 including the conditions when correcting for phase distortions (see Refs. 4, 5, and 11).

THE OCCURRENCE AND DEVELOPMENT OF INDUCED CONVECTIVE MOTIONS

When the velocity of a medium motion is much less than the speed of sound and the pressure is constant the motion of viscous heat-conducting gas (liquid) is described by the set of Navier–Stokes equation in the Boussinesq approximation[1]:

$$\frac{\partial \mathbf{V}}{\partial t} + (\mathbf{V}\nabla_\perp)\mathbf{V} = -\frac{1}{\rho}\nabla p + \nu\Delta_\perp \mathbf{V} + \beta \mathbf{g}(T - T_0),$$

$$\frac{\partial T}{\partial t} + (\mathbf{V}\nabla_\perp)T = \chi\Delta_\perp T + \frac{\alpha I_0}{\rho C_p} f(r); \qquad (1)$$

$$\operatorname{div} \mathbf{V} = 0,$$

where $p = p - \rho_0(\mathbf{gr})$ is the Boussinesq quasi-pressure, i.e., the pressure minus hydrostatic one; V, T are the velocity and temperature in the medium; T_0, ρ_0, p_0 are the temperature, density, and pressure well away from the beam; $\chi = k_m/\rho C_p$ is the coefficient of thermal diffusivity; k_m is the coefficient of thermal conductivity; C_p is the specific heat at constant pressure; ν is the modulus of kinematic viscosity; β is the coefficient of thermal expansion; α is the absorption coefficient; I_0 is the intensity at the beam axis; $f(r)$ is the function, characterizing the laser beam intensity profile of the radius a.

Detailed analysis of the set of equations (1) and numerical simulation have been carried out in the Ref. 1 for the dimensionless velocities in the form of Peclet numbers $V_p = \mathrm{Pe} = Va/\chi$, being the measure of the ratio between the molecular and convective heat transfer in the flow and the Reynolds number $V_R = \mathrm{Re} = Va/\nu$, determining the hydrodynamic character of the medium motion (laminar flow at $\mathrm{Re} < 2320$, turbulent flow at $\mathrm{Re} > 10000$). As regards the hydrodynamics of the process the dimensionless velocity is expressed through Reynolds number. The velocity, expressed through the Peclet number, characterizes the degree of thermal blooming of a laser beam in a convective flow penetrating it. To do this, dimensionless parameters are being introduced: $\mathbf{r} = \mathbf{r}/a$ are the coordinates, $t_\chi = \chi t/a^2$, $t_\nu = \nu t/a^2$ is time; $T_p = \beta g(T - T_0)a^3/\chi^2$, $T_R = \beta g(T - T_0)a^3/\nu^2$ are the temperatures, $q_p = \alpha\beta g l_0\, a^5/(\rho_0\, C_p\, \chi^3)$, $q_R = \alpha\beta g l_0\, a^5/(\rho_0\, C_p\, \nu^3)$ are the dimensionless thermal complexes, characterizing the density of internal heat sources. The physical characteristics of the medium are characterized by the Prandtl similarity number $\mathrm{Pr} = \nu/\chi$, determining the ratio of the inertia and gravity forces in a homogeneous field.

To analyze qualitatively the development of convective motions, induced by laser radiation, we have earlier carried out,[1] dimensional analysis of equations for the dimensionless velocities V_R, V_p. This analysis involves a comparison of different terms of these equations that characterize the behavior of the corresponding process as well as determination of the role of different mechanisms with the isolation of the basic ones that support this process. As the liquid is believed to be incompressible, $\operatorname{div}\mathbf{V} = 0$ and its velocity far outside the beam equals zero, the field of velocities may be assumed to be solenoidal. Therefore the pressure is not involved in the analysis.

In the case of a laser beam propagation along a horizontal path the dimensional analysis enables us to

0235-6880/98/11 1006-11 $02.00

classify the three regimes of convection: weak, moderate and developed. The conditions for these regimes occurrence and the convection velocities are given in Table I.

The numerical simulations dealt with the problem on convective motion caused by absorption of laser radiation in an extended cell of a square-shaped cross section under the following assumptions:

– laser radiation propagates parallel to the cell axis;

– the cell is long enough for the effects of its ends to be neglected;

– the laser radiation heating is uniform along the axis, i.e., the absorption of laser radiation is weak.

The numerical simulation is made for the cell with a square-shaped cross section of the size R, equal to $R/a = 10$. The calculations have been done using dimensionless values of heat release $q_{R_1} = (R/a)^5 q_R$, the temperature $T_{R_1} = (R/a)^3 T_R$, the velocity $V_{R_1} = (R/a) V_R$, and the time $t_R = t\nu/R^2$.

TABLE I. Convection velocities under different regimes and different media.

Type of the medium	Convection regime		
	Weak V_R, $V_p \ll 1$	Moderate $V_R \ll 1$, $V_p \gg 1$	Developed V_R, $V_p \gg 1$
Viscous liquids Pr $\gg 1$	$V_c^w = C_{11} \dfrac{\alpha\beta g a^4 I_0}{k_m \nu}$ at $V_p < C_{11}^2$; $0 < q_p < \mathrm{Pr}\, C_{11}$	$V_c^m = C_{12} \left(\dfrac{\alpha\beta g a^3 I_0}{\rho_0 C_p \nu}\right)^{1/2}$ at $C_{11}^2 < V_p < \mathrm{Pr}\,(C_{13}^3/C_{12})$; $(C_{11}/C_{13}^3)\,\mathrm{Pr} < q_p < \left(\dfrac{C_{13}}{C_{12}}\right)^6 \mathrm{Pr}$	$V_c^d = C_{13} \left(\dfrac{\alpha\beta g a^2 I_0}{\rho_0 C_p}\right)^{1/3}$ at $V_p > \mathrm{Pr}\left(\dfrac{C_{12}^3}{C_{13}}\right)$; $q_p > \mathrm{Pr}^3 \left(\dfrac{C_{13}}{C_{12}}\right)^6$
Gases Pr ≈ 1	$V_c^w = C_{21} \dfrac{\alpha\beta g a^4 I_0}{k_m \nu}$ at $0 < V_p < \left(\dfrac{C_{23}}{C_{21}}\right)^{1/2}$; $0 < q_p < \left(\dfrac{C_{23}}{C_{21}}\right)^{3/2}$	No explicit mode	$V_c^d = C_{23} \left(\dfrac{\alpha\beta g a^2 I_0}{\rho_0 C_p}\right)^{1/3}$ at $V_p > \left(\dfrac{C_{23}}{C_{21}}\right)^{1/2}$; $q_p > \left(\dfrac{C_{23}}{C_{21}}\right)^{3/2}$

TABLE II. Values of the proportionality coefficients and characteristic times of setting of the convective regime in a long cell of square-shaped cross section.

Type of the medium	Convection regime		
	Weak V_R, $V_p \ll 1$	Moderate $V_R \ll 1$, $V_p \gg 1$	Developed V_R, $V_p \gg 1$
Viscous liquids Pr = 20	$q_1 = 7.2\cdot10^{-4}$; $\tau_T = \tau_\nu = a^2/\chi$; $q_R < 10^{-2}$–10^{-3}	$q_2 = 3\cdot10^{-2}$; $\tau_T = a/V_k$, $\tau_\nu = a^2/\nu$, $10^{-2} < q_R < 10^4$	$q_3 = 0.46 - V_m$, $q_3 = 0.23 - V_0$; $\tau_T = \tau_\nu = a/V_c$, $q_R > 10^4$
Gases Pr ≈ 1	$q_1 = 3.5\cdot10^{-5}$; $\tau_T = a^2/\chi$, $\tau_\nu = a^2/\nu$, Pr < 1, $\tau_\nu = a^2/\chi$, Pr ≥ 1, $q_R = 1$–10		$q_3 = 0.46 - V_m$, $q_3 = 0.23 - V_0$; $\tau_T = \tau_\nu = a/V_c$
Plasma Pr ≈ 0.05	$q_1 = 1.7\cdot10^{-6}$; $\tau_T = a^2/\chi$, $\tau_\nu = a^2/\nu$; $q_R = 10^2$	$\tau_T = a^2/\chi$, $\tau_\nu = a/V_c$	$q_3 = 0.46 - V_m$, $q_3 = 0.23 - V_0$; $\tau_T = \tau_\nu = a/V_c$

The numerical simulation conducted confirmed existence of three convection regimes. It also enabled determining the values of proportionality coefficients as well as the times of establishing the steady state convection regime and the boundaries of heat release parameters (Table II, where V_m is the convection velocity at the maximum point; V_0 is the velocity at the beam axis).

The properties characteristic of the occurrence and development of convective motion in different regimes are as follows.

1. Under regime of weak convection the structure of convective motion keeps practically the same with only the flow intensity smoothly varying towards its value in the steady state regime. Isotherms are close to the circular-shaped ones. The heat transfer from the heat release zone is realized as a result of heat conductivity. For the viscous media and gases with the Prandtl number Pr ≥ 1 the time of establishing the steady state regime of temperature gradients $\tau_T = a^2/\chi$ and velocity $\tau_\nu = a^2/\chi$ is only determined by heat conductivity ~ k_m. For the media with the Prandtl number Pr < 1 (gases and plasma) the time $\tau_T = a^2/\chi$ is defined by thermal conductivity, and $\tau_\nu = a^2/\nu$ by the medium viscosity.

The process of establishing the temperature and velocity in the regime of weak convection on the beam axis T_0, V_0, and the periphery T_a, V_a is illustrated in Fig. 1. The coefficient C_1 depends on the number Pr, while the ratio $C_1(\mathrm{Pr})/\mathrm{Pr}$ being constant.

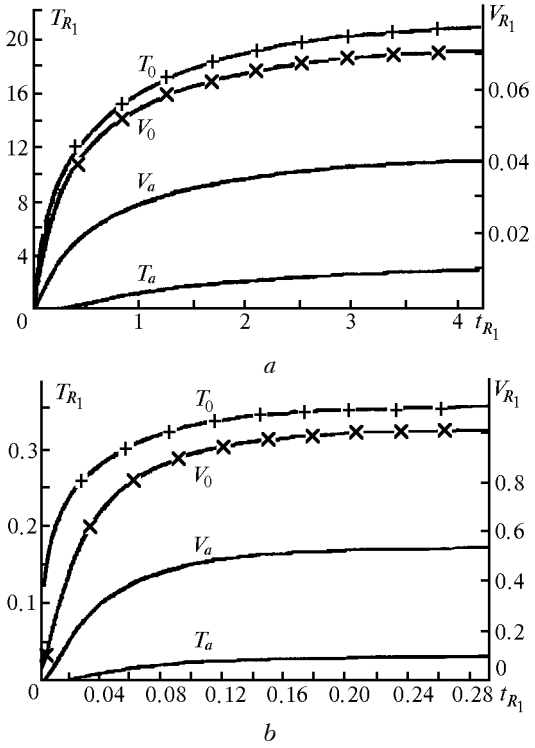

FIG. 1. Establishment of temperature and velocity in the regime of weak convection at $q_{R_1} = 10^2$ *for the Prandtl number* Pr = 20 *(a);* Pr = 1 *(b) (Ref. 1).*

2. At a moderate-rate convection the isotherms are markedly distorted, under the effect of the velocity field, with the temperature and velocity maxima being shifted upward, and significant horizontal temperature gradients appear in the zone above the beam axis. Convective motion is very important in heat transfer. The development process is a rapidly damped autooscillating process. The cause of autooscillations is the following. The convective flow in this regime lags behind the temperature. Therefore local heating of the medium occurs.

As a result, the buoyancy force value exceeds the equilibrium value, and the fluid picks up to speed higher than that under steady state conditions. This, in its turn, leads to a decrease of temperature, and then the velocity of motion decreases. At the beam periphery the autooscillating process is weaker than at its center. The time required for establishing the steady state regime of temperature and velocity is defined by the Prandtl number $\mathrm{Pr} = \nu/\chi$. For the viscous fluids ($\mathrm{Pr} >> 1$) $\tau_T = a/V_c$; $\tau_\nu = a/\nu$. For gases ($\mathrm{Pr} << 1$) the regime of moderate convection is manifests itself implicity and $\tau_T = a/\chi$, $\tau_\nu = a/V_c$. When estimating the settling time the rule $\tau_\nu > \tau_T$ is effective. Figure 2 illustrates the establishment of temperature and velocity in the regime of moderate convection on the beam axis, T_0, V_0, and on its periphery, T_a, V_a.

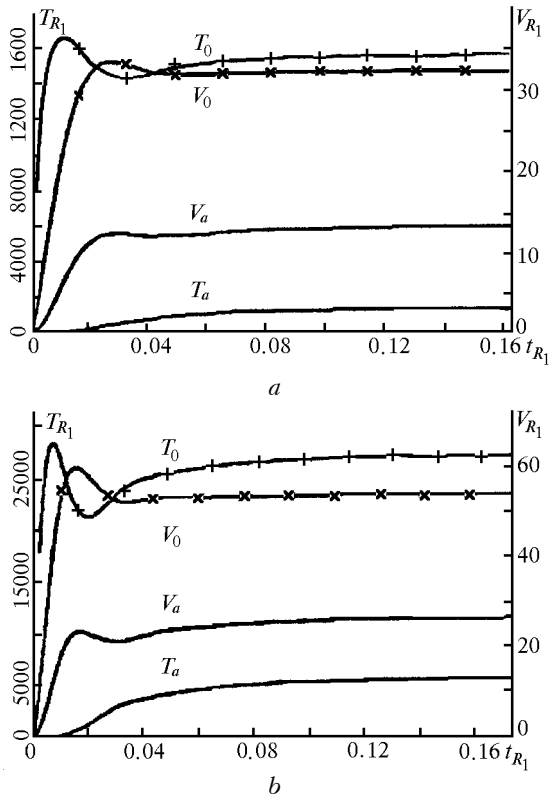

FIG. 2. Establishment of temperature and velocity in the regime of moderate convection at $q_{R_1} = 10^7$ *for the Prandtl number* Pr = 20 *(a);* Pr = 1 *(b) (Ref. 1).*

3. In the regime of a developed convection the proportionality coefficient C_3 does not depend on the Prandtl number Pr and for the velocity on the beam axis V_0 it equals 0.23, while being 0.46 at the maximum V_m. Isotherms, being initially symmetric, are strongly distorted under the effect of the velocity field, and above the beam axis the isotherms take the mushroom shape due to a strong vertical stream of the hot medium and finite size of the cell volume. The shift of maxima of temperature and velocity does not depend on the heat release parameter. The time of settling the steady state regime of temperature and velocity is only determined by the convection velocity. The autooscillating character of the setting time is more clearly defined. The secondary eddies occur, which point to the turbulence origin. The process of settling the temperature and velocity in the regime of a developed convection on the beam axis, T_0, V_0, and on its periphery, T_a, V_a, is illustrated in Fig. 3.

The peculiarities characteristic of the stages of the onset and establishment of the convective and temperature fields in the regime of a developed convection in a round cell of radius $R = 10a$ are illustrated with the data in Figs. 4 and 5, obtained by numerical integration of equations of the type (2) (see

Ref. 2). The structure of the convective heat flux is of a "dipole" shape, and, as it develops, we notice the shift of maximum vorticity upwards and the circular motion is found to be compressed against the upper part of the cell. The temperature field that initially has a circular symmetry takes a strongly complicated structure and becomes nonuniform. The rate of establishment of the convective flux lags behind the temperature.

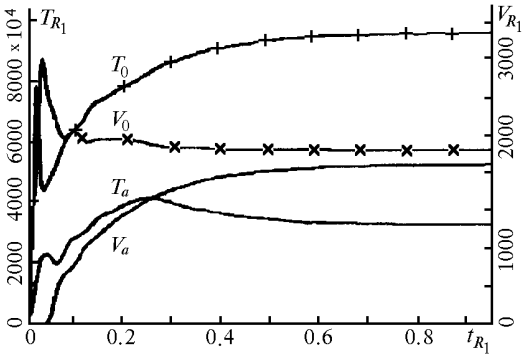

FIG. 3. Establishment of temperature and velocity in the regime of developed convection at $q_{R_1} = 10^{12}$ *for the Prandtl number* Pr = 1 *(Ref. 1).*

In Ref. 3 similar calculations made for the cell of a square-shaped cross section of a larger size ($R/a = 50$) showed that the structure of temperature field becomes smoother and has no typically dipole view. However, this does not result in an essential change in the beam shape as compared with that in the cell of $R/a = 10$ size.

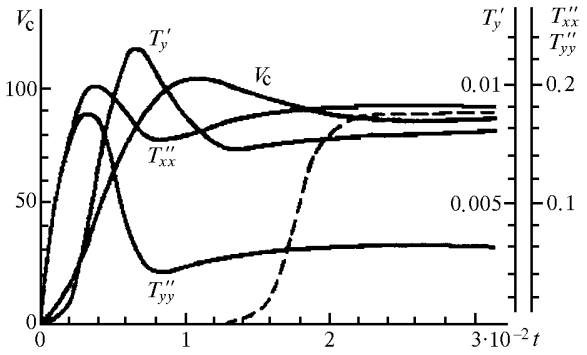

FIG. 4. Time behavior, on the beam axis, ($x = y = 0$*) of the convection velocity* $V_R = -\mathrm{d}\psi/\mathrm{d}x$*, vertical temperature gradient* T'_y*, the values of* $T''_{xx} = \partial^2 T/\partial.^2$*,* $T''_{yy} = \partial^2 T/\partial 3^2$*, characterizing the localization of temperature on the axes at the value* $q_{R_1} = 2\cdot10^7$*. The heat flux through the cell boundary is shown by the dashed line. Here the dimensionless temperature is* $T = T\nu\rho q_p/\alpha I_0 R^2$ *(Ref. 3).*

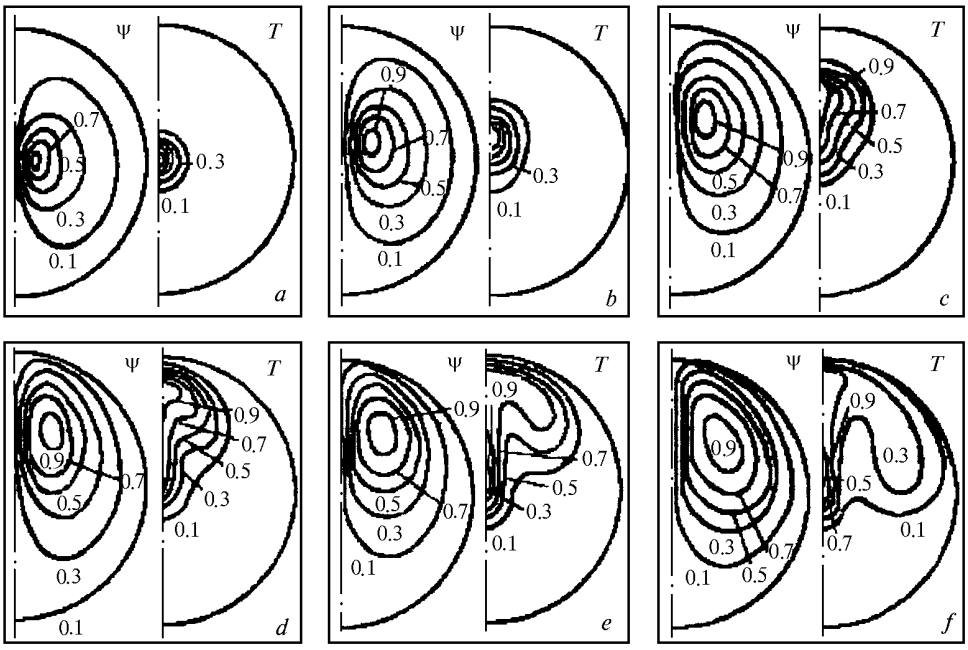

FIG. 5. The isotherms normalized to the maximum value $T = \text{const}$ *and the lines of current* ψ *of the induced convection in cylindrical (*$R/a = 10$*) gas cell (*Pr = 0.7*) at different moments in time after turning on the heat source (Ref. 2).*

The steady state velocity of convection in a gas cell (Fig. 6) first grows in proportion to the source power $V_c = \beta g \alpha a^2 p/\pi\rho C_p \chi\nu^2$ (the regime of weak convection) then it turns into the regime of a developed

convection $V_c = (g\alpha p/\pi\rho C_p)^{1/3}$ without an explicity manifested part of a moderate convection.

In the numerical experiment (the crosses on the straight line *2*) the time moment when the temperature gradient on the beam axis reaches its maximum is chosen as time of the regime establishment, and the line *2* has been calculated by formula $\tau_c \approx \eta(2=/V_c) \sim (\alpha p)^{1/3}$ with the scaling factor $\eta = 2$.

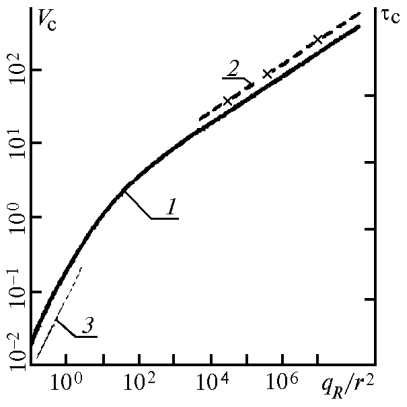

FIG. 6. The dependence of the steady state velocity of induced convection V_c (curve 1), calculated in a single-mode approximation, on the source power for the gas cell ($r = R/a = 10$, Pr = 0.7); curve 2 shows the dependence of time of the induced convection development $\tau_c \approx \eta(2=/V_c) \sim (\alpha p)^{1/3}$ on the source power; the straight line 3 denotes $V_c \sim q_R/r^2 \sim \alpha p$ (Ref. 2).

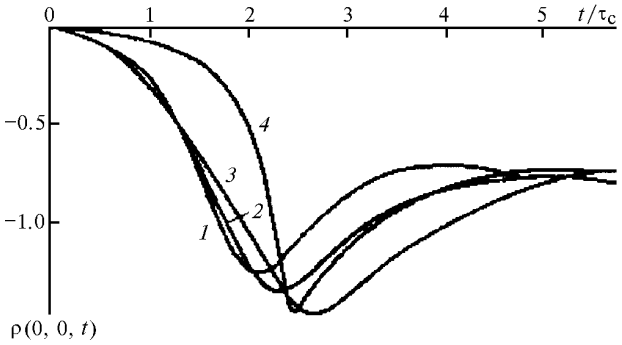

FIG. 7. Variation of the density disturbances at the center of a ring beam ($a/a_v = 3$) as a function of time: in an open space Re = 56, Pe = 42 *(1); in a horizontal tube of a square-shaped cross section of the size* 6.4*a,* Re = 56, Pe = 42 *(2); in a narrower tube of the size* 4*a,* Re = 56, Pe = 42 *(3); in the less heat-conducting and viscous gas in a tube of the size* 6.4*a,* Re = 343, Pe = 244 *(4).*

In Ref. 6 the solution of the set of equations (1) has been achieved using discrete Fourier transform. Figure 7 from Ref. 6 shows the results on variation of the disturbed medium density on the beam axis as a function of time, that coincide, by the curve shapes, with the experimental results on the displacements of a beam image presented below.

LASER RADIATION PROPAGATION UNDER CONDITIONS OF SELF-INDUCED CONVECTION

In Refs. 4, 5, and 11 one may find a description of numerical simulations of thermal blooming of a single-mode and partially coherent laser beam that is being propagated through a medium under conditions of self-induced convection. The three-dimensional problem of hydrodynamics reduces to a set of two-dimensional problems, the number of which coincides with the number of discrete steps along the longitudinal variable z. In each of the planes z = const the motion of viscous heat-conducting gas is described by the set of the Navier–Stokes equations in the Boussinesq approximation (1), written in the variables "functions of current ψ – vorticity ωB (see Refs. 4 and 5)

$$\frac{\partial\omega}{\partial t} + (\mathbf{V}\nabla_\perp)\omega = \frac{1}{\mathrm{Re}}\Delta_\perp\omega + \frac{q_R}{\mathrm{Re}^3}\frac{\partial T}{\partial x},$$

$$\frac{\partial T}{\partial t} + (\mathbf{V}\nabla_\perp)T = \frac{1}{\mathrm{Pr\ Re}}\Delta_\perp T + f(r); \qquad (2)$$

$$\Delta_\perp\psi = -\omega.$$

In the set of Eqs. (2) the operators $\Delta_\perp$ and $\nabla_\perp$ are taken along the transverse coordinates x, and y; and the gas velocity V has two components V_x, V_y, $V_z = 0$, that are connected with the flow function by the relationships $V_x = \partial\psi/\partial y$, $V_y = \partial\psi/\partial x$, $\omega = \frac{\partial V_y}{\partial x} + \frac{\partial V_x}{\partial y}$. For the dimensionless parameters, entering into the set of Eqs. (2), the commonly accepted normalization is used by the characteristic velocity of the medium motion under conditions of developed convection V_c and the time $\tau_c = =/V_c$:

$$V_c = \frac{\nu q_R^{1/3}}{a} = \left(\frac{\alpha\beta g a^2 I_0}{\rho C_p}\right)^{1/3}. \qquad (3)$$

The function $f(r)$, that characterizes the laser beam intensity profile at the medium entrance, is set as a Gaussian function for a single-mode radiation and as the Gaussian statistics of the mutual coherence function in the multimode regime.

The propagation of a light beam is described by a dimensionless equation for the complex slowly varying amplitude of a light wave.

In the numerical experiment the random realization of the beam amplitude at the medium entrance was set by the spatial distributions of real and imaginary parts of the field. For numerical simulation of random fields we used the method of frequency sampling with a subsequent averaging over 100 realizations. In the experiment we determined the such beam parameters as the dynamic structure of nonlinear distortions and their mode composition, spatial

structure, characterized by the spectral criterion J_Ω, the limiting possibilities of compensating for phase distortions in a multimode beam.

The spectral criterion J_Ω characterizes the relative part of the total power P, concentrated in a given solid angle Ω, and is determined by the expression

$$J_\Omega = \frac{1}{4\pi P} \iint \Omega\,(k_x,\, k_y)\,|\,\tilde{E}\,(k_x,\, k_y,\, z_0,\, t)\,|^2\,\mathrm{d}k_x\,\mathrm{d}k_y, \quad (4)$$

where k_x, k_y are the wave vector projections on the plane perpendicular to the direction of beam propagation; $\tilde{E}$ is the spectrum of a complex wave amplitude.

In the numerical experiment the solid angle Ω was selected so that in the absence of nonlinear distortions the diffraction limited value of the criterion J_Ω equaled 0.5.

The investigations in Refs. 4 and 5 have shown that at different values of the heat release parameter behavior of the lowest aberrations is very similar, and they mainly differ in the amplitude and time of establishing the steady state temperature field (Table III).

TABLE III. Steady state values of the expansion coefficients for the output phase and the times of establishing the steady state temperature field at different q_R values.

q_R	Re	τ_{st}/τ_c	Tilt a_2	Defocusing a_3	Astigmatism a_4	Coma a_7	Coma a_9
10^3	10	30	1.56	1.1	−0.31	−0.29	0.25
10^4	21.5	15	3.39	2.37	−0.49	−0.75	0.75
10^5	46.5	7.8	7.88	5.74	−0.79	−1.77	1.59

In this case the amplitudes of all the modes in the range of values studied, $q = 10^3$–10^5, vary practically proportional to the number Re (Fig. 8) whose value under conditions of a developed convection equals $\mathrm{Re} = q - V_R$.

Equations of the regression lines, describing the dependence of amplitudes of the expansion coefficients of phase a_c on the Re number, are as follows:

$=_2 = -0.252 + 0.174\ \mathrm{Re};$

$=_3 = -0.267 + 0.128\ \mathrm{Re};$

$=_4 = -0.193 - 0.013\ \mathrm{Re};$

$=_7 = 0.119 - 0.0406\ \mathrm{Re};$

$=_9 = -0.078 + 0.0362\ \mathrm{Re}.$

The time variation of amplitudes of the expansion coefficients of the wave phase a_c and the spectral criterion J_Ω at the modal compensation of the beam phase distortions is presented in Figs. 9 and 10 (Refs. 4 and 5).

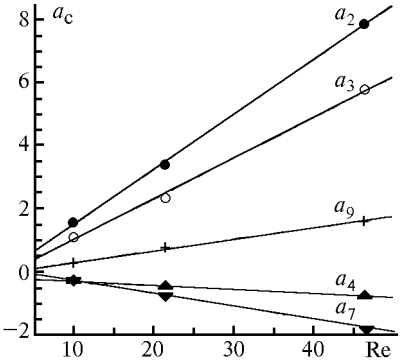

FIG. 8. The dependence of steady state values of the expansion coefficients for phase a_c on the Reynolds number. Designations of modes correspond to those in Table III.

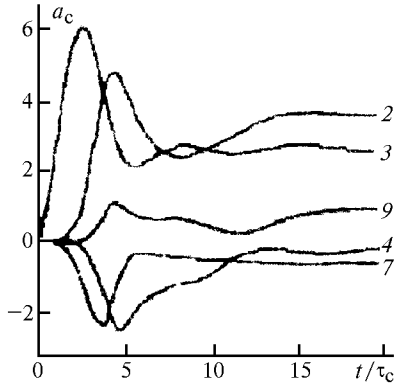

FIG. 9. Time distortions of the expansion coefficients of the beam phase at the cell output over the lowest aberrations at $q_R = 10^4$. The figures at curves correspond to the numbers of modes from Table III (Ref. 4).

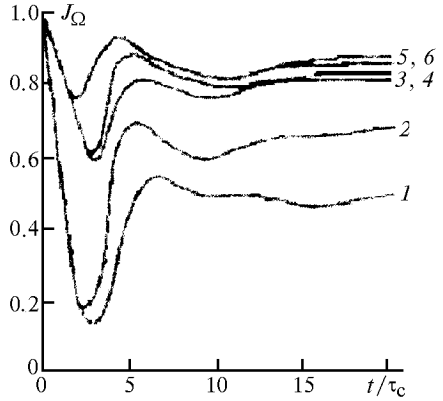

FIG. 10. Time dependences of spectral criterion J_Ω at modal compensation of the beam phase distortions at $q_R = 10^4$. Curve 1 shows the data without any compensation; curve 2 – with the compensation for the phase tilt; curves 3, 4 – with the compensation using the 1st and 2nd order modes; curves 5, 6 – with compensation using the 1st, 2nd and 3rd order modes (Ref. 4).

Such a behavior of the coefficients of phase expansion is caused by the variation of pressure, temperature and the velocity of the convective motion (compare Figs. 4, 7, and 9). At the first stage $t/\tau_c < 2$ the beam defocusing a_3 takes place due to the medium heating. Then the developed convective flux distorts the symmetric structure of temperature field that results in a decrease of the defocusing a_3, to the beam displacement toward the flow a_2, and distortion of the beam shape a_4, a_7, a_9. At $t/\tau_c \approx 3$–5, when the flow velocity reaches its maximum the distortions and beam displacement are also maximal. Later on the temperature and velocity of the flow decrease and, as a result, the beam distortions and displacement also decrease. As a result of autooscillations the steady state distorted phase front is established.

The results of numerical experiments on the mode correction of nonlinear phase distortions[5] are shown in Fig. 10. It is evident that the main contribution to the distortions comes from the tilt (in a steady state regime the exclusion of this aberration leads to a 40% improvement of the spectral criterion); the effect of the second order aberrations is slightly below (a 15% improvement of the criterion) and the removal of coma leads to a 10% increase in the spectral criterion.

At the same time, as analysis of the results of relative contribution of different regimes to the steady beam phase (Table IV) indicates, at the growth of the heat release parameter q_R, the spatial structure of phase distortions becomes more complicated. This manifests itself in an increase of the fraction of higher aberrations, which are not removed by means of the modal corrector.

TABLE IV. Relative contribution of different modes to the steady state beam phase at the cell output, estimated by the spectral criterion $J_{\Omega x}$

q_R	Tilt, %	2nd order mode, %	3rd order mode, %	Higher modes, %
10^3	45.8	31.7	5.8	16.7
10^4	36.1	28.2	8.7	27.0
10^5	7.2	20.6	10.3	61.9

The numerical solution of the set of equations (2) for investigating the dynamics of a convective flow in the cell of a square-shaped cross section under conditions of correction for the beam phase distortions has been performed in Ref. 11. To solve the equations, an implicit scheme, which is a version of the method of variable directions in combination with the fast Fourier transform (FFT) method, was used. We have analyzed the rms deviation of the temperature field in time, which determined the rms phase deviation accurate to a constant factor. It is shown that with the increase of absorbed energy the residual distortions of the field of temperatures and phase, i.e., the spectrum of phase distortions shifts toward the higher-order aberrations. The efficiency of a segmented corrector practically does not differ from that of a modal corrector that provides correcting for all aberrations.

The experimental investigations of non-steady state regime under conditions for the establishment of self-induced convection have been carried out for fluids[8,12] and gas[6,7] cells.

In Ref. 8 the studies were made of the shift of centers of gravity of the image of the impact ($\lambda_m = 0.488$ μm; the radius $a_m = 4$ mm) and sounding ($\lambda_s = 0.6328$ μm; the radius $a_s = 0.4$ mm) laser beams in the cell of $25 \times 25 \times 35$ cm size filled with water pigmented with fuchsin, having the absorption coefficient $\alpha = 0.06$ cm^{-1} at λ_m. The shifts of center of gravity were measured in the focal plane of the objective, located following the cell, using the dissector tracking system. The impact beam has previously been collimated with an optical system in a medium without absorption.

The state of the medium is described by the following parameters:

the parameter of separation

$$q = \frac{\beta g \alpha P a_m^3}{\pi \rho C_p \nu^3} = (4\text{–}70); \qquad (5)$$

the velocity of convection,[9] cm·s^{-1},

$$V_c = \left(\frac{\beta g \alpha P\, a_m}{16\rho\, C_p\, \nu} \right)^{1/2} = (0.22\text{–}0.92)\ ; \qquad (6)$$

the Reynolds number

$$\mathrm{Re} = a_m\, V_c/\nu = (0.87\text{–}3.7);$$

the Peclet number

$$\mathrm{Pe} = a_m\, V_c/\chi = (6.2\text{–}26.4);$$

the time of convection, *s*,

$$\tau_c = a_m/V_c = (18.2\text{–}4.3);$$

the time of the thermal diffusion, s

$$\tau_\chi = =_m^2/\chi = 115;$$

the typical length of a thermal lens, cm,

$$L_t = \left(-\frac{\partial n}{\partial T} \frac{\alpha P}{\pi\rho\, C_p\, V_c\, a_m^3\, n} \right)^{1/3} = (180\text{–}87),$$

where $P = \pi a^2$ is the radiation source power.

The values of these parameters point to the fact that in the experiment the regime of moderate convection ($\mathrm{Re} \sim 1$, $\mathrm{Pe} \gg 1$) has been realized.

The characteristic shifts of the centers of gravity of the impact and sounding beams are given in Fig. 11. The abscissa shows time normalized to the time of convection τ_c, calculated for the conditions of moderate convection in a fluid ($\mathrm{Pr} \approx 7$), realized in this experiment.

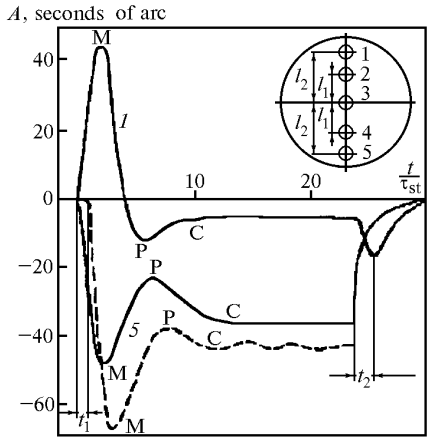

FIG. 11. Recording of the image displacements of the impact (dashed line) and sounding beams (solid curves). In the upper part of the figure the positions of sounding beams, are shown in the cross-section of the impact beam together with the distances l_1 = 2.8 mm, l_2 = 4 mm *(Ref. 8).*

Figure 12 shows the three-dimensional image of the surface, describing the shift of the center of gravity of the image of the impact beam, normalized to the steady state value depending on time t and the parameter of heat release q. The figure has been constructed based on the mean values of all the realizations and gives a clear view of the function behavior. The figures show that the displacement of the image of the beam center of gravity in time, reflecting the behavior of the wave front tilt, by its form is identical to the calculated one (see Fig. 9, curve *2*) for the conditions of a developed convection. In the experiment we analyze the amplitudes of shifts A and times of reaching the characteristic points of the process: A_m, t_m denote the maximum shift (M); A_p, t_p denote the point of transition to the stationary state (P); $A_{0.5}$, $t_{0.5}$ denote the level 0.5 A_m; A_{st} is the amplitude of a stationary state (C); t_1 is the time from the start of the effect up to the onset of the convective motion (start of the shift of the beam image). We did not manage to determine the time of establishing the steady state regime in the experiment with an acceptable error because in the majority of cases after the point of bending (P) the oscillatory regime is observed with a small trend toward the shift increase. Note, however, that the start of oscillations and the establishment of the steady state regime begins at t_c = 90–125 s for all q values. The amplitude at the time t_c was taken as A_{st}. This fact indicates that under a moderate convection regime the time of establishing the stationary state is, to a greater degree, defined by the thermal conductivity $\tau_\chi = a_m^2/\chi$ = 115 s.

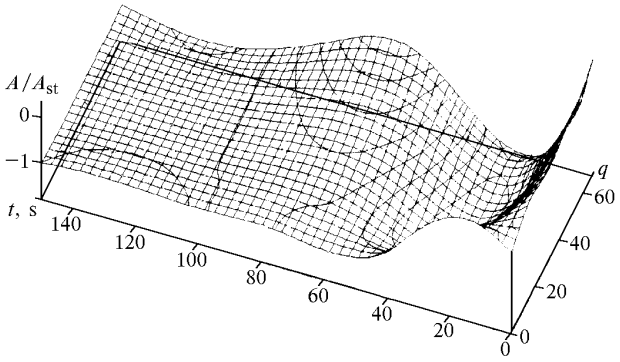

FIG. 12. The dependence of the time t and the parameter of heat release q of the image displacements of the acting laser beam A, normalized to the steady state value A_{st} *(Ref. 8).*

The dependence of the analyzed values on the heat release parameter q are presented in Figs. 13–16.

Curves in Figs. 13 and 14 were calculated by the method of least squares with the use of the "OriginB program, and their equations are given in Table V.

The results of investigations revealed that under conditions of the setting on of self-induced convection at $q < 5$, Re ~ 1 the center of gravity of the beam image is being smoothly shifted from the initial position to the steady state one. The amplitudes of maximum shift and at the transition point A_m, A_p are close to the steady state ones (see Fig. 13) and the setting on time of a stationary state is close to $\tau_\chi = a_m^2/\chi$ = 115 s. The start of the image shift toward the convective flux in time is close to the times $\tau_c \le 16$ s, τ_v = 16 s. Such a behavior of the shift of center of gravity of the beam image points to the fact that at Re ≤ 1 the regime of a weak convection is realized.

At $q > 5$, Re > 1 the regime of a moderate convection is realized, and the image shift is of the form of quickly damped autooscillations and three typical stages are observed:

1. At the first stage, starting with switching on the source and to the time $t_1 \sim \mathrm{Re}^{-1.5} \sim q^{-0.75}$ the beam thermal defocusing occurs due to the medium heating by the absorbed energy.

TABLE V. Equations of the regression lines for the data presented in Fig. 13 and 14.

$A_{0.5}$	A_m	A_p	A_{st}	t_1	$t_{0.5}$	t_m	t_p	τ_c
$1.45q^{0.74}$	$2.84q^{0.77}$	$3.2q^{0.56}$	$2.73q^{0.66}$	$54.7q^{-0.79}$	$66q^{-0.52}$	$88q^{-0.41}$	$76 - 0.55q$	$36q^{-0.5}$
$4.9\ \mathrm{Re}^{1.48}$	$9.3\ \mathrm{Re}^{1.54}$	$9.7\ \mathrm{Re}^{1.12}$	$7.8\ \mathrm{Re}^{1.28}$	$14.5\ \mathrm{Re}^{1.58}$	$28\ \mathrm{Re}^{-1}$	$45\ \mathrm{Re}^{-0.82}$	$88 - 13q$	$16\ \mathrm{Re}$

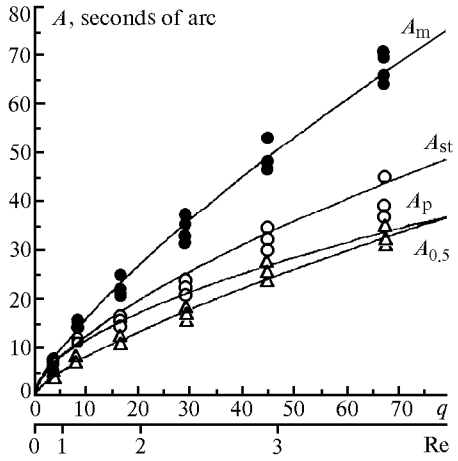

FIG. 13. The amplitude of shift of the impact beam depending on the heat release parameter q (the Reynolds number Re*): at a point of maximum shift (A_m), in the stationary state (A_{st}), at a transition point of the process (A_p without the experimental points), and at the level of* $0.5A_m$ *($A_{0.5}$) (Ref. 8).*

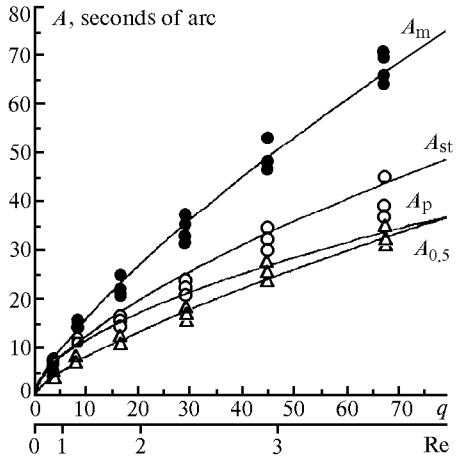

FIG. 14. The dependence of time of reaching characteristics points: the maximum shift (t_m), the transition point (t_p), at the level of $0.5A_m$ *($t_{0.5}$), the onset of a convective motion (t_1), and the reference line of the convection time* τ_c *(dashed curve), on the heat release parameter q (the number* Re*) (Ref. 8).*

The image shifts are insignificant and occur both upwards and downwards. Then the developed convective flow distorts the homogeneous temperature field resulting in significant vertical gradients of temperature and the shift of the beam image toward the flow. The time t_1 is close to the times τ_c, τ_ν at the Reynolds numbers $\mathrm{Re} \le 1$ and rapidly decreases with increasing power deposit (see Fig. 14).

2. At the second stage, at $t_p > t > t_1$, the beam image is shifted down (toward the convective flow), reaches maximum (point M) at $t_m \sim \mathrm{Re}^{-0.8} \sim q^{-0.4}$, then it returns up, going through the stationary state and reaches a transition point (P), completing the first, most complicated period of damped oscillations (see Fig. 11, Table V). A peculiarity of the transition point is in the fact that the time when it is reached weakly depends on the power deposit q and is (0.7–0.4) τ_χ or (4–10) τ_c. The time, when the shifted amplitude equals the half of maximum amplitude, decreases proportional to the Reynolds number $t_{0.5} \sim \mathrm{Re}^{-1} \sim q^{-0.5}$ and coincides very closely with the time of convection $\tau_c \sim \mathrm{Re}^{-1}$. The ratio $t_{0.5}/\tau_c \approx 1.7$ and remains constant under the measurement conditions (see Fig. 14, Table V).

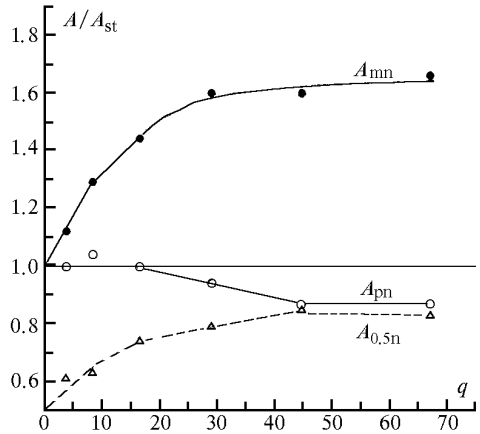

FIG. 15. The dependence of the amplitudes A, normalized to the steady state value A_{st}*, at points of maximum shift,* A_{mn}*, bending point,* A_{pn}*, at the level of* 0.5 *of maximum shift,* $A_{0.5n}$ *on the heat release parameter q, (Ref. 8).*

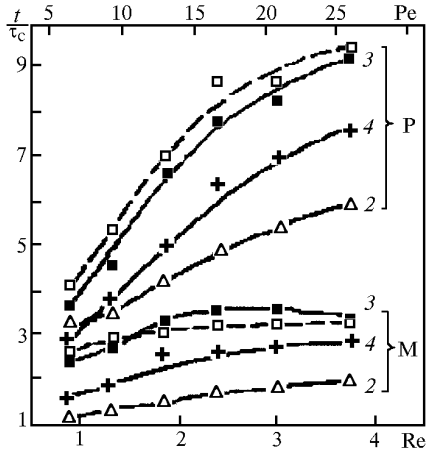

*FIG. 16. The dependence of the time of reaching the maximum shift (*M*) and the transition point (*P*) by the impact (dashed curves) and sounding beams (solid curves) normalized to* τ_c *on the Reynolds number* Re *(the Peclet number* Pe*). The positions of sounding beams in the cross section of an impact one is the same as in Fig. 11 (Ref. 8).*

The value of t_m is 2.5–3 τ_c (see Fig. 16) that is close to the data of numerical simulation for the conditions of developed convection in gases (see Fig. 9) and the time of reaching maximum values of wind

velocity under conditions of a moderate convection (see Fig. 2). The absolute values of the amplitudes of the oscillation process grow with the increase in q (see Fig. 13 and Table V), however, the amplitudes normalized to the steady state value, saturate at $q > 50$, Re > 3 (see Fig. 15).

3. The third stage. This stage denotes the establishment of the steady state regime, and starts at $t \sim 100$ s $\approx \tau_\chi$ and it is characterized by the smooth transition to $A_{st} \sim q^{0.65} \sim \mathrm{Re}^{1.3}$. In this case, at Re > 3, we observe the small-amplitude oscillations about the steady state value.

The investigations of the image shift of sounding beams in the channel of the impact beam, determined by the induced field of the refractive index show that:

– the field of the refractive index in the channel cross section is inhomogeneous both in time of stabilization and in the integral quantity of the gradient; the character of shifts of a sounding beam from the "windward" side of the channel is similar to that of the shift of the impact beam; the establishment of the steady state shift on the "leeward" side of the channel occurs in the opposite phase with the impact beam;

– the sounding beams on the "windward" side of the channel describe the process of the amplitude shift of the impact beam most accurately, while in time this process is better represented in the central part of the channel (see Fig. 15);

– the amplitude and directions of the shift of sounding beams at the channel tilt depend on the absorbing power and the angle between the impact and sounding beams.[12]

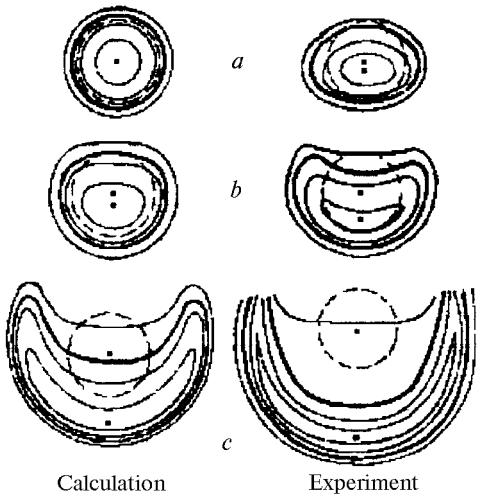

FIG. 17. A comparison between the theoretical and experimental isophotes at steady-state thermal blooming of the Gaussian beam: (a) $\alpha = 0.31$ m^{-1}, Re = 2.15, $V_c = 1.1$ cm/s, $\tau_c = 0.27$ s, $p = 1$ atm; *(b)* $\alpha = 0.22$ m^{-1}, Re = 4.83; $V_c = 1.25$ cm/s, $\tau_c = 0.24$ s, $p = 2$ atm; *(c)* $\alpha = 0.66$ m^{-1}, Re = 16.7, $V_c = 1.72$ cm/s, $\tau_c = 0.174$ s, $p = 5$ atm (*Ref. 6*).

The numerical calculations of the intensity distribution over the cross section of a beam, propagating under conditions of self-induced convective motion, have been done in a large number of papers (see, e.g., Refs. 1–3, 6, and 7). As an example, Figure 17 gives a comparison between theoretical and experimental isophotes[6, 7] under steady state regime and different conditions of propagation.

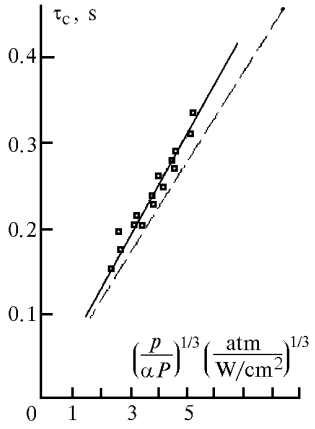

FIG. 18. A comparison between the calculated dependence of the convection time $\tau_c = a/V_c$ *(dashed line) and the experimentally measured time* t_m, *determined as a moment of maximum deviation of laser beam at the gas cell output (solid line) (Ref. 7).*

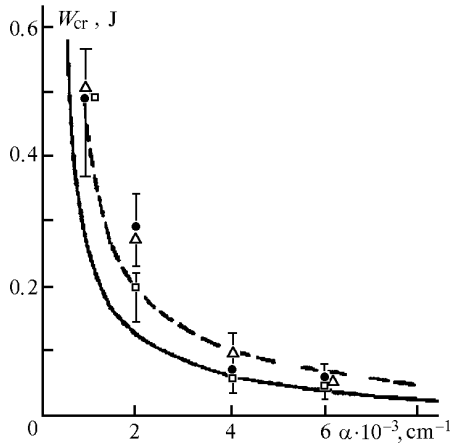

FIG. 19. A comparison of theoretical (solid curve) and experimental (dashed curve) dependences of critical energy W_{cr} *of thermal self-defocusing on the absorption coefficient of a gas medium (Ref. 7).*

In Ref. 7 we have described the experimental investigations of the effect of induced convective motion of a gas on the thermal blooming of a CO_2-laser beam of 0.3 cm radius in an air-filled horizontal cell at pressures from 1 to 10 atm with a minor admixture of the propane-butane mixture. This has made it possible

to vary the conditions of propagation using the two independent parameters: the absorption coefficient α and the pressure p. In the experiment we measured the beam parameters (the amplitude and the time of shift of a point of maximum intensity, the beam radius, the amount of critical energy of thermal self-defocusing), that were compared with the results calculated in the non-aberrational approximation[10] for steady state conditions. Some of these results are shown in Figs. 18 and 19.

The basic conclusions drawn in Ref. 7 are as follows.

1. The convective motion, if appeared, leads to strong asymmetric distortion of the beam cross section configuration; the formulae, based on the non-aberration approximation, overestimate the values of the beam deviation.

2. Under conditions of a developed convection the time of nonlinear distortions development is determined by the time of the convective heat transfer (see Fig. 18). The ratio between the time when the maximum beam deviation is reached and the reference time of the convection development is a constant value $t_m/\tau_c \approx 1.2$. The convection velocity may be calculated by the following formula:

$$V_c = \left[\frac{g\alpha P}{2\pi\rho\, C_p\, Tp} \right]^{1/3},$$

where T is the temperature, K; p is the pressure. The authors explain this difference by the uncertainty in choosing the characteristic beam scale a, when deriving formula for V_c. Note that all the subsequent results of numerical simulation and measurements[5, 6] have shown this ratio to be $t_m/\tau_c = 2–3$.

3. The critical amount of energy of thermal self-defocusing at local inertial nonlinearity is in a good agreement with the theoretical estimate (see Fig. 19). Theoretical values were calculated by the formula $W_{cr} = \rho C_p \chi^2 / n 2\pi\alpha$, где $n \sim p$ is the refractive index of the medium. The threshold value of the absorbed power for a significant convection to occur is $\alpha p \le 0.01$ W·cm^{-1} for a beam of ~ 1 cm diameter.

REFERENCES

1. V.M. Gordienko, "*The investigation of thermal blooming of* CO_2*–laser radiation in gas media*,B Cand. Phys.-Math. Sci. Dissert., Moscow (1976), 152 pp.
2. V.A. Petrishchev, L.V. Piskunova, V.I. Talanov, and R.E. Erm, Izv. Vyssh. Uchebn. Zaved., Radiofizika **24**, No. 2, 161–171 (1981).
3. B.P. Gerasimov, T.G. Elizarova, A.P. Sukhorukov, Zh. Tekh. Fiz. **63**, No. 9, 1696–1705 (1983).
4. I.E. Tel'pukhovskii and S.S. Chesnokov, Atmos. Oceanic Opt. **6**, No. 12, 857–860 (1993).
5. I.A. Chertkova and S.S. Chesnokov, Atm. Opt. **3**, No. 2, 108–113 (1990).
6. A.N. Kucherov, Atmos. Oceanic Opt. **6**, No. 12, 864–868 (1993).
7. V.A. Petrishchev, N.M. Sheronova, and V.E. Yashin, Izv. Vyssh. Uchebn. Zaved., Radiofizika **28**, No. 7, 963–974 (1975).
8. V.M. Sazanovich and R.Sh. Tsvyk, Atmos. Oceanic Opt. **6**, No. 12, 869–872 (1993).
9. D.K. Smith, Proc. IEEE **65**, No. 12, 59–103.
10. V.A. Aleshkevich and A.P. Sukhorukov, Pis'ma Zh. Eksp. Teor. Fiz. **30**, No. 12, 112 (1970).
11. V.P. Lukin and B.V. Fortes, Atm. Opt. **3**, No. 12, 1182–1185 (1990).
12. A.B. Il'in, A.P. Larichev, V.M. Sazanovich, and R.Sh. Tsvyk, Atmos. Oceanic Opt. **5**, No. 1, 33–37 (1992).